Towards UAV-Based Ultra-Wideband Multi-Baseline SAR Interferometry

Victor Mustieles-Perez[#*1], Sumin Kim[#2], Christina Bonfert[†3], Gerhard Krieger[*#4], Michelangelo Villano[#5]

[#]Microwaves and Radar Institute, German Aerospace Center (DLR), Germany

[*]Institute of Electrical-Electronic-Communications Engineering, Friedrich-Alexander-Universität (FAU), Germany

[†] Institute of Microwave Engineering, Ulm University, Germany

[1]victor.mustieles@fau.de, {[2]sumin.kim, [4]gerhard.krieger, [5]michelangelo.villano}@dlr.de, [3]christina.knill@uni-ulm.de

***Abstract* — Unmanned Aerial Vehicle (UAV)-based synthetic aperture radar (SAR) systems enable very accurate and cost-effective monitoring of local areas with unprecedentedly short revisit intervals. This paper discusses specific aspects that arise in the context of UAV-based multi-baseline SAR interferometry (InSAR) for the generation of digital elevation models (DEMs). UAV-based SAR systems are often characterized by a large fractional bandwidth, thus the common narrowband spaceborne approximations yield inaccurate predictions for the geometric decorrelation and the critical baseline. A new formulation is proposed and validated by simulation. Based on the theoretical analyses, a multi-baseline InSAR experiment is planned. The DEM performance analysis shows that large baselines enable height accuracies in the sub-decimeter range, where geometric and volume decorrelation become the limiting factors. This paves the way to height measurements with unprecedented accuracy for multiple applications.**

***Keywords* — cooperative SAR, interferometry, multistatic SAR, SAR, UAV**

I. Introduction

Unmanned aerial vehicle (UAV) technology has advanced significantly in recent years, making UAVs particularly attractive. The key developments include increased payload capacity, improved positioning systems and flying stability, extended integration with custom software for user-defined trajectory planning, and cost reductions [1]. In the field of remote sensing, UAVs have attracted interest for the detection of buried objects, such as landmines, by means of ground penetrating radars and synthetic aperture radar (SAR) processing. They benefit from long wavelengths to penetrate the ground, allowing as well for retrieving soil, ice or snow properties, which also makes them interesting for planetary exploration [2] [3]. More recently, UAVs have also gained interest for Earth observation because they offer advantages over traditional space- and airborne missions. UAVs, on the other hand, are easy-to-deploy and cost-effective systems that enable very accurate and frequent monitoring of local areas. This makes them ideal for studying local-scale dynamic processes using densely sampled time-series. Furthermore, flying configurations and available bandwidths are generally less constrained [4]. These features make UAVs valuable for scenarios where traditional systems have restricted capabilities. UAVs are also very attractive for the demonstration of spaceborne concepts, in terms of multi-platform configurations and future wideband spaceborne systems [5].

The capabilities of UAV-based SAR systems can be exploited to a further extent using multiple cooperative platforms, which coherently receive the backscattered echoes from multiple angles. They are currently being investigated within the KoRaTo project [6].

Across-track interferometric SAR (InSAR) exploits the phase shift between two complex SAR images of the same scene acquired from slightly different positions to retrieve topographic information in the form of digital elevation models (DEMs) [7] [8]. The two SAR images can be acquired at different times in monostatic mode (repeat-pass InSAR) or simultaneously using two spatially separated antennas in bistatic mode (single-pass InSAR). The latter is to be preferred, since undesired changes in the scene might occur even over short periods and compromise the quality of the resulting DEM.

The height accuracy of the DEM improves as the distance between the antennas (or geometrical baseline), which calls for the use of distinct platforms, which, however, need to be synchronized. The height accuracy is also affected by the interferometric coherence, i.e., the complex cross-correlation between the two SAR images. The main coherence loss (or decorrelation) sources are the limited signal-to-noise ratio (SNR), the temporal decorrelation (in the case of repeat-pass InSAR), and the geometric baseline decorrelation [9]. The latter is due to the fact that the scene is imaged from different incident angles, poses a limit to the baseline, and motivates the exploitation of multiple baselines (multi-baseline InSAR).

The aim of this paper is to pose the basis to obtain DEMs with unprecedented height accuracy using multi-baseline InSAR. Section II presents a novel formulation for the geometric baseline decorrelation in wideband InSAR systems and Section III addresses a DEM performance analysis which accounts for the peculiarities of UAV-based wideband systems.

II. Novel Formulation of the Geometric Baseline Decorrelation for Wideband InSAR Systems

Spaceborne InSAR models usually assume a long-range geometry and narrowband signals [7] [10]. Thus, their validity has to be verified for the short-range wide-fractional-bandwidth case of the UAVs. A closer analysis reveals that the impact of having a short-range geometry is minor. Relative errors in the

calculation of the height of ambiguity, the critical baseline and the impact of localization uncertainty in the DEM are typically smaller than 3%. Therefore, spaceborne approximations still hold for narrowband signals and narrow swaths, i.e. 20% of UAV flying altitude. In contrast, large swaths, i.e., a large variation of the incidence angle between near and far range, and large fractional bandwidths results in non-negligible effects One of its main induced errors is the geometric baseline decorrelation, which is discussed in the following for a repeat-pass InSAR scenario.

A. Derivation of the geometric baseline decorrelation

Let us consider the interferometric geometry represented in Fig. 1, where $P_i, i \in \{1,2\}$ are the positions of the radar platforms 1 and 2, respectively, R_i are the slant-ranges, θ_i are the angles of incidence, H is the height of platform 1, β is the angle between both platforms, and B is the baseline which can be decomposed in the parallel, $B_{\parallel}$, and the perpendicular, $B_{\perp}$, components. Note that a flat terrain is considered for simplicity. To derive the geometric baseline decorrelation the signal model from [11] and a similar procedure are considered. The down-converted signal in platform 1 may be approximated as

$$s_1\left(\frac{2u}{c}\sin\theta_1\right) = r(y_0+u)e^{-j\left(\frac{2w_0}{c}\right)(z_{01}+u\sin\theta_1)} * w\left(\frac{2u}{c}\sin\theta_1\right) \quad (1)$$

where $*$ denotes convolution, $z_{01} = \sqrt{H^2+y_0^2}$, u is the displacement from y_0 in the y-axis, $w_0 = 2\pi f_0$ is the central frequency, $r(y)$ is the terrain reflectivity and $w\left(\frac{2u}{c}\sin\theta_1\right)$ is the impulse response of the system. Note that the impulse response of the system does not depend on z_{01}, which only introduces a phase shift to the received signal. The signal model is valid for both pulsed and frequency-modulated continuous-wave (FMCW) radars. Defining $\tau = u\frac{2}{c}$, it yields

$$s_1(\tau\cdot\sin\theta_1) = r\left(y_0+\frac{\tau c}{2}\right)e^{-j\left(\frac{2w_0}{c}\right)z_{01}}e^{-jw_0(\tau\cdot\sin\theta_1)} * w(\tau\cdot\sin\theta_1). \quad (2)$$

Then, Fourier transforming (2) with respect to τ, it results in

$$S_1(w) = R(w+w_0\sin\theta_1)e^{-j\left(\frac{2w_0}{c}\right)z_{01}}W\left(\frac{w}{\sin\theta_1}\right), \quad (3)$$

where $R(w)$ and $W(w)$ are the Fourier transforms of the terrain reflectivity, $r\left(y_0+\frac{\tau c}{2}\right)$, and the system impulse response, $w(\tau)$, respectively. Similarly, the signal corresponding to the second platform can be written as

$$S_2(w) = R(w+w_0\sin\theta_2)e^{-j\left(\frac{2w_0}{c}\right)z_{02}}W\left(\frac{w}{\sin\theta_2}\right). \quad (4)$$

The Fourier transforms of both signals show that the imaged reflectivity is shifted by $w_0\sin\theta_i$, while the imaged bandwidth is stretched by a factor $1/\sin\theta_i$. For narrowband signals, the shrinkage of the imaged bandwidth can be neglected, but this is not the case for wideband signals. It can be shown that the frequency shift and bandwidth shrinkage are equivalent to a model that projects the imaged frequencies of the transmitted

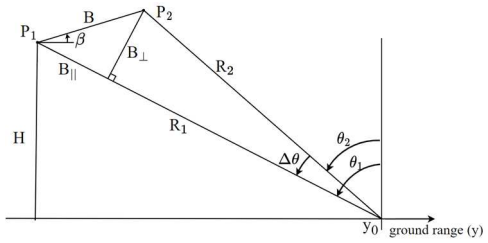

Fig. 1. Cross-track InSAR geometry.

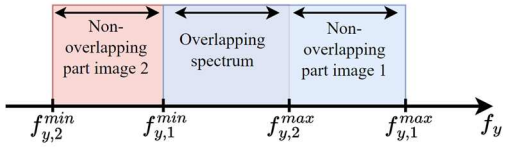

Fig. 2. Ground-range projected spectra of the two SAR images. Overlapping and non-overlapping regions are indicated.

spectra on the ground [7] [12]. If the projected frequencies are denoted as f_y, then the projected frequencies for the platforms 1 and 2 are given by, respectively, $f_{y,1} = f\sin\theta_1$ and $f_{y,2} = f\sin\theta_2$. The greater the overlap between the imaged ground reflectivity spectra of the two SAR images, the higher the coherence between them. Thus, the geometric correlation coefficient may be computed considering common and non-common spectrum parts as proposed in [10]. Under the assumption of rectangular spectra and for $\theta_1 > \theta_2$, the projected spectra as well as the overlapping parts look as depicted in Fig. 2, where $f_{y,i}^{max}$ and $f_{y,i}^{min}$ are the projections of the maximum and minimum transmitted frequencies for each of the platforms. The coherence may then be written as

$$\gamma_{Rg} = 2\frac{f_{y,2}^{max}-f_{y,1}^{min}}{\left[\left(f_{y,1}^{max}-f_{y,1}^{min}\right)+\left(f_{y,2}^{max}-f_{y,2}^{min}\right)\right]}. \quad (5)$$

Note that a factor of 2 must be considered between the common and non-common parts because the latter appear only in one of the two SAR images. Substituting the values of all frequencies, (5) can be expressed as

$$\gamma_{Rg} = \frac{1}{B_p}\frac{(2+B_p)\sin(\theta_1-\Delta\theta)-(2-B_p)\sin\theta_1}{\sin\theta_1+\sin(\theta_1-\Delta\theta)} \quad (6)$$

for $\Delta\theta < \Delta\theta_{crit}$, where $B_p = B_{Rg}/f_0$ is the fractional bandwidth of the system, $\Delta\theta = \theta_1 - \theta_2$ is the interferometric angle, $\Delta\theta_{crit}$ is the interferometric angle corresponding to the critical baseline, and B_{Rg} is the system bandwidth. Note that $\Delta\theta$ cannot be directly approximated as $\Delta\theta \approx B_{\perp}/R_1$ like in spaceborne systems because the flying formation has a notable influence, since the condition $B_{\perp} \ll R_1$ does not hold. With reference to the geometry in Fig. 1, it can be instead written as

$$\Delta\theta = \arctan\left(\frac{B_{\perp}}{R_1-B_{\parallel}}\right). \quad (7)$$

The critical baseline, $B_{\perp,crit}$, is the baseline for which both SAR images become completely uncorrelated. From the result of the geometric decorrelation of (6), it may be derived imposing:

$$\gamma_{Rg}\big|_{B_{\perp,crit}} = 0. \quad (8)$$

Analogous derivations can be made for the bistatic case. The frequency shift and, therefore, the baseline decorrelation are smaller than for the monostatic case, and are exactly half when very similar incident angles are assumed, thus in agreement with the spaceborne case [10].

The expression of the baseline decorrelation obtained in (6) is validated with the results of simulations and compared with the approximation used in spaceborne scenarios given by [9]

$$\gamma_{Rg\ Space} = \begin{cases} 1 - \frac{B_\perp}{B_{\perp,crit\ Space}}, & B_\perp < B_{\perp,crit\ Space} \\ 0, & B_\perp \geq B_{\perp,crit\ Space} \end{cases} \quad (9)$$

where the critical baseline may be expressed as

$$B_{\perp,crit\ Space} = \frac{\lambda R_1 B_{Rg}}{c} \tan\theta_1. \quad (10)$$

The comparison is shown in Fig. 3. The parameters of the UAV system considered are $f_0 = 2.5$ GHz, $B_{Rg} = 3$ GHz [3], with a platform altitude of $H = 100$ m. The curves will scale for different flying heights, obtaining the same coherence for larger or smaller baselines. It becomes clear that the coherence is notably overestimated when increasing the baseline if the spaceborne approximation is used. This will cause a mismatch between predicted and obtained interferometric performances when using relatively large baselines. Given that the baseline decorrelation obtained notably differs from the spaceborne approximation, the critical baseline varies accordingly resulting in smaller values. This outcome is relevant because the largest usable baseline does not increase linearly with the bandwidth as expected from the spaceborne approximation in (10).

B. *Further options*

Filtering the SAR signals to a common bandwidth to avoid decorrelation at the expense of resolution is used to improve the final performance. The non-common ground spectral components are filtered out. The two passband filters used are defined depending on the frequency shift and with the same bandwidth [12]. In a wideband scenario, the bandwidth shrinkage needs to be considered, thus both filters have to be of different bandwidths. Furthermore, in a geometry with a large variation of the incidence angle across the swath, different frequency shifts and spread factors occur. The implications of forming an interferogram from two SAR images with different bandwidths therefore need further investigation.

III. DEM Performance Analysis and Experimental Demonstration

A. *Objectives*

A measurement campaign for multi-baseline repeat-pass interferometry has been planned and performed. Its objectives are to demonstrate the theoretical results. The capabilities of absolute ranging methods [13] [14] will be analyzed as well. A variety of measurement configurations in terms of different platform heights and interferometric baselines has been defined. The acquisitions in this first experiment are performed in a repeat-pass strip-map mode, and serve as a preparation of future multi-baseline single-pass InSAR.

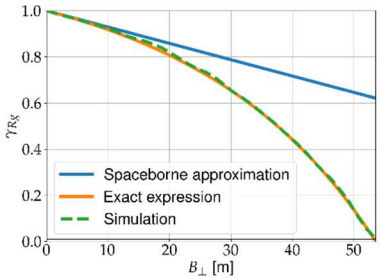

Fig. 3. Comparison between geometrical decorrelation obtained with the spaceborne approximation, the derived exact expression and the simulation.

Table 1. System parameters assumed in the DEM performance analysis.

Parameter	**Value**	**Parameter**	**Value**
Frequency band	1 - 4 GHz	Drone speed	2 m/s
Transmit power	10 dBm	Duty cycle	0.8
System noise figure	5 dB	Antenna gain	6 dBi
Additional losses	3 dB	Antenna mounting	45°
Pulse repetition frequency	1 kHz	Beamwidth in azimuth	50°
Signal quantization	12 bits	Beamwidth in elevation	60°

B. *Interferometric performance analysis*

A detailed DEM performance analysis has been conducted for each of the configurations that are planned to be tested. The analysis is similar to [8], but adapted to the specific case of the UAVs. The UAV-mounted radar system considered is detailed in [3], [4]. To compute the SNR, the system parameters from Table 1 and the sigma nought model for soil and rock, VV, L-band from [15] are assumed. The main contribution to volume decorrelation is considered to be ground penetration, which is computed using the model in [16] for a mid-moisturized soil. The geometric baseline decorrelation is modelled as presented in Section II. Range and azimuth ambiguities are negligible due to the low flying altitudes of the UAVs and the low speeds, respectively. Instead, right-left ambiguities have to be considered due to the wide antenna beamwidth. The geometric and volume decorrelations are the most important decorrelation sources, in contrast to spaceborne systems, where the finite SNR is the limiting factor. Both of them have a greater impact on the steepest incident angles and large baselines.

The impact of possible additional degradations has also been studied. The flying accuracy of the UAVs is in the order of a meter due to GNSS localization. A swath overlapping of 30% and a margin with respect to the nominal trajectory are defined to account for this. Its impact is more considerable for low flying altitudes. The accuracy of the positioning system is in the order of 1 cm. Because of it, the DEM may have systematic displacement or tilt smaller than 2 cm and 2 cm/m, respectively, and height errors lower than 10 cm, which are reduced to less than 3 cm for large baselines. To account for a possible underestimation of the interferometric coherence, an additional 10 % margin in the interferometric phase errors is considered, which results in height errors smaller than 2 cm.

The predicted height accuracies of the DEM are in the sub-decimeter range for an independent post-spacing of 0.25 m × 0.25 m. Fig. 4 shows the predicted height accuracy for the

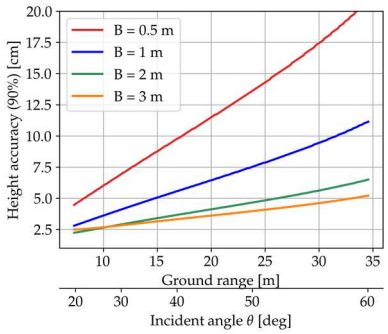

Fig. 4. Predicted height accuracy (90%) for a flying altitude of 20 m, different horizontal baselines, and an independent post-spacing of 0.25 m × 0.25 m.

aforementioned UAV system, a flying altitude of 20 m above ground level and different horizontal baselines. These curves do not include the previously discussed additional degradations. In general, the height accuracy improves as the baselines increase. However, the height accuracy deteriorates for steep incident angles and very large baselines due to the notable effects of the geometric and volume decorrelation. Phase unwrapping is challenging for such accuracies. However, we can use multiple baselines and absolute ranging. In the experiment design, it has been shown that, due to the large fractional bandwidth, the achievable accuracy with absolute ranging methods may be comparable to interferometry and hence they can be used to help in phase unwrapping. A similar performance was obtained as well for platform heights up to 40 m. Thus, the instantaneous coverage can be notably increased while keeping a great height accuracy if the transmit power is sufficient. The swath width goes from 6.5 m for H = 5 m to 40 m for H = 30 m, considering $\theta_i \in [20°, 60°]$.

The acquisitions are designed to have some overlaps so it will be possible to check that everything fits together. For further verification, a ground truth of some areas will be acquired using a three-dimensional laser scanner.

C. *Test site*

The test site selected for the experiment contains some topography variations and portions of different types of soil with different properties, i.e., grass, clay, gravel and sand. Furthermore, a small artificial scene consisting of a metallic mesh with randomly distributed gravel on top is set to ensure very reduced penetration. It will also allow to isolate the volume decorrelation from the rest of the contributions to the coherence loss. The metallic mesh avoids the penetration. The gravel is needed to avoid the periodicity of the mesh and the specular reflection of the radar signal on it. The artificial scene will be set as well following a desired topography.

IV. Conclusion and Outlooks

This paper poses the basis for UAV-based multi-baseline SAR interferometry. It has been shown that decorrelation models derived previously for narrowband spaceborne scenarios overestimate the coherence and the critical baseline in wideband InSAR systems. Therefore, an exact formulation is proposed, which is validated by simulation and will be corroborated experimentally. Unprecedented DEM height accuracies in the sub-decimeter range are feasible with UAVs.

While this work focuses on interferometry of surfaces for which no penetration is desired, wide fractional bandwidth of UAVs can also be used to invert the trend of the interferometric coherence versus frequency and retrieve the three-dimensional structure of semi-transparent media, thereby opening a new opportunity for tomographic SAR imaging [17].

Acknowledgment

This work was partially funded by the Deutsche Forschungsgemeinschaft (DFG, German Research Foundation) GRK 2680 – Project-ID 437847244.

References

[1] P. Hügler *et al.*, "Radar Taking Off: New Capabilities for UAVs," in *IEEE Microwave Magazine*, vol. 19, no. 7, pp. 43-53, Nov.-Dec. 2018.

[2] A. Grathwohl *et al.*, "Taking a Look Beneath the Surface: Multicopter UAV-Based Ground-Penetrating Imaging Radars," in *IEEE Microwave Magazine*, vol. 23, no. 10, pp. 32-46, Oct. 2022.

[3] R. Burr *et al.*, "UAV-Borne FMCW InSAR for Focusing Buried Objects," in *IEEE Geoscience and Remote Sensing Letters*, vol. 19, pp. 1–5, 2022.

[4] R. Bahnemann *et al.*, "Under the sand: Navigation and localization of a micro aerial vehicle for landmine detection with ground-penetrating synthetic aperture radar," *Field Robotics*, 2021.

[5] M. Villano *et al.*, "Potential of Multi-Static SAR Systems for Earth Monitoring and Their Demonstration Using Swarms of Drones," *IGARSS 2023, Pasadena, CA, USA, 16-21 July 2023.*

[6] (2023) The KoRaTo website. [Online]. Available: https://www.uni-ulm.de/in/korato/

[7] R. Bamler and P. Hartl, "Synthetic aperture radar interferometry," *Inverse Problems*, vol. 14, Art. no. 4, Aug. 1998.

[8] P. A. Rosen *et al.*, "Synthetic aperture radar interferometry," *Proceedings of the IEEE*, vol. 88, Art. no. 3, Mar. 2000.

[9] G. Krieger *et al.*, "TanDEM-X: A Satellite Formation for High-Resolution SAR Interferometry," *IEEE Transactions on Geoscience and Remote Sensing*, vol. 45, Art. no. 11, Nov. 2007.

[10] H. A. Zebker and J. Villasenor, "Decorrelation in interferometric radar echoes," in *IEEE Transactions on Geoscience and Remote Sensing*, vol. 30, Art. no. 5, 1992.

[11] C. Prati and F. Rocca, "Improving slant-range resolution with multiple SAR surveys," *IEEE Transactions on Aerospace and Electronic Systems*, vol. 29, Art. no. 1, 1993.

[12] F. Gatelli, A. M. Guamieri, F. Parizzi, P. Pasquali, C. Prati, and F. Rocca, "The wavenumber shift in SAR interferometry," *IEEE Transactions on Geoscience and Remote Sensing*, vol. 32, Art. no. 4, Jul. 1994.

[13] R. Bamler and M. Eineder, "Accuracy of Differential Shift Estimation by Correlation and Split-Bandwidth Interferometry for Wideband and Delta-k SAR Systems," *IEEE Geoscience and Remote Sensing Letters*, vol. 2, Art. no. 2, Apr. 2005.

[14] G. Krieger and A. Moreira, "Multistatic SAR satellite formations: potentials and challenges," in *Proceedings. 2005 IEEE International Geoscience and Remote Sensing Symposium, 2005. IGARSS '05.*, 2005, vol. 4, pp. 2680–2684.

[15] Fawwaz Ulaby, M. Craig Dobson, and J. L. Alvarez Perez. *Handbook of Radar Scattering Statistics for Terrain*. Norwood, MA: Artech House, 1989

[16] M. T. Hallikainen, F. T. Ulaby, M. C. Dobson, M. A. El-rayes and L. -k. Wu, "Microwave Dielectric Behavior of Wet Soil-Part 1: Empirical Models and Experimental Observations," in *IEEE Transactions on Geoscience and Remote Sensing*, vol. GE-23, no. 1, pp. 25-34, Jan. 1985.

[17] S. Kim, V. Mustieles-Perez, G. Krieger, and M. Villano, "Three-Dimensional Structure Inversion Through Wide Fractional Bandwidth, UAV-Based SAR Interferometry," *IRS 2023, Berlin, Germany, 24-26 May 2023.*